DIVISION S-1—SOIL PHYSICS

Calibration of a Two-Dimensional Root Water Uptake Model

J. A. Vrugt, J. W. Hopmans,* and J. Šimunek

ABSTRACT

Although solutions of multidimensional transient water flow can be obtained by numerical modeling, their application may be limited in part as root water uptake is generally considered to be one-dimensional only. The objective of this study was to develop and test a two-dimensional root water uptake model, which can be incorporated into numerical multidimensional flow models. The two-dimensional uptake model is based on the model by Raats, but is extended with a radial component. Subsequently, the root water uptake model was incorporated into a two-dimensional flow model, and root water uptake parameters were optimized, minimizing the residuals between measured and simulated water content data. Water content was measured around a sprinkler-irrigated almond tree (*Prunus laurocerasus* M.J.Roem) for a 16-d period at 25 locations, following irrigation. To calibrate the flow and root water uptake model, a genetic algorithm (GA) was used to find the approximate global minimum of the optimized parameter space. The final fitting parameters were determined using the Simplex algorithm (SA). With the optimized root water uptake parameters, simulated and measured water contents during the 16-d period were in excellent agreement, with R^2 values generally ranging between 0.94 and 0.99 and a root mean squared error (RMSE) of 0.015 m^3 m^{-3}. The developed root water uptake model is extremely flexible and allows spatial variations of water uptake as influenced by nonuniform (drip irrigation) and uniform water application patterns.

Fᴿᴏᴍ ᴀ ʜʏᴅʀᴏʟᴏɢɪᴄᴀʟ ᴘᴇʀsᴘᴇᴄᴛɪᴠᴇ, water uptake by root systems and their spatial distribution can largely control water fluxes to the atmosphere and the groundwater (Canadell et al., 1996). For an improved understanding of the magnitude of these fluxes, accurate esti-mates of the temporal and spatial root water uptake patterns are needed. Quantification of root water extraction rates also contributes to an improved understanding of chemical fluxes in the vadose zone in both ecological and hydrological studies (Somma et al., 1998), as well as their control by vegetation. Water uptake by rooting systems can control the timing and the amount of chemical pollutant loadings to the groundwater through elimination of preferential flow patterns of water and chemicals, or by regulation of absorption of nutrients or trace elements, thereby reducing their concentration levels in the deep vadose zone or groundwater (Clothier and Green, 1994). Moreover, the rhizosphere might be responsible for accelerated breakdown of organic chemicals by biodegradation (Walton and Anderson, 1990).

Actual root water uptake not only depends on the root distribution and its functioning, but also on soil water availability and salinity. In addition to water stress in periods of low water availability, root water uptake is also reduced when concentrations of soluble salts exceed plant-specific threshold values (Homaee, 1999). In irrigated soils, particularly in arid and semiarid regions, plants are generally subjected to both salinity and water stress. In these regions, soil and water management practices are based on maintaining a favorable soil water content and salinity status in the root zone, thereby minimizing periods of water stress while controlling leaching to minimize salinity stress.

The influence of plant–root systems on water and chemical movement can be better understood using soil water simulation models, provided that accurate spatial and temporal root water uptake distributions are included (Musters and Bouten, 1999; Musters, 1998). The

J.A. Vrugt, Institute for Biodiversity and Ecosystem Dynamics, University of Amsterdam, The Netherlands, Nieuwe Prinsengracht 130, Amsterdam, 1018 VZ; J.W. Hopmans, Hydrology Program, Dept. Land, Air and Water Resources (LAWR), University of California, Davis, CA 95616, USA; J. Šimunek, USDA Salinity Laboratory, University of California, Riverside, CA 95207, USA. Received 18 Nov. 1999 *Corresponding author (jwhopmans@ucdavis.edu).

Abbreviations: CIMIS, California Irrigation Management Information System; CV, coefficient of variation; GA, genetic algorithm; RMSE, root mean squared error; SA, simplex algorithm.

most common approach for modeling root water uptake in unsaturated flow is based on introducing a sink term, S, in the Richards equation (Whisler et al., 1968; Molz, 1981; Clausnitzer and Hopmans, 1994) describing transient multidimensional water flow:

$$\frac{\partial \theta}{\partial t} = \nabla[K\nabla(h - z)] - S \quad\quad [1]$$

where θ is the volumetric water content ($L^3 L^{-3}$); K is the unsaturated hydraulic conductivity ($L\ T^{-1}$); h (L) is the soil water pressure head; z (positive downwards) denotes the gravitational head (L) (to be included for the vertical flow component only); and S is the volumetric sink term ($L^3 L^{-3} T^{-1}$), being a function of both space and time. However, application of multidimensional flow models requires the spatial characterization of root water uptake as well. Available uptake models are largely limited to one dimension only (Feddes et al., 1974; Molz, 1981; Jarvis, 1989), describing variations in water uptake with soil depth while allowing for reduction in uptake by soil water stress. Exceptions are the two-dimensional models proposed by Neuman et al. (1975) and Warrick et al. (1980). However, their application to describe different types of root distributions is fairly limited. Most recently, Coelho and Or (1996) proposed bivariate gaussian root distribution density functions (normal, semilognormal and lognormal) as parametric models for the description of root water uptake patterns of drip-irrigated row crops.

It is the objective of this study to develop a flexible multidimensional root water uptake model to be integrated in the two-dimensional HYDRUS-2D flow code (Šimunek et al., 1999). Furthermore, the root water model was calibrated using the spatial distribution of water contents around a sprinkler-irrigated almond tree during a 16-d monitoring period.

MATERIALS AND METHODS
Root Water Uptake Model

As basis of the proposed root water uptake model, we used the exponential model by Raats (1974),

$$\beta(z) = \frac{1}{\lambda}e^{-\frac{z}{\lambda}} \quad\quad [2]$$

where $\beta(z)$ is the spatial root water uptake distribution with depth (L^{-1}); λ (L) is selected such that at depth λ the cumulative root water uptake is 63% of total uptake over the whole root zone; and z is the depth in the soil profile ($z \geq 0$). The proposed model excludes λ, but includes three additional parameters

$$\beta(z) = \left[1 - \frac{z}{z_m}\right]e^{-\frac{p_z}{z_m}|z^* - z|}; \quad z \geq 0 \quad\quad [3]$$

where $\beta(z)$ denotes the dimensionless spatial root distribution with depth; z_m is the maximum rooting depth (L); and p_z (-) and z^* (L) are empirical parameters. These parameters were included to provide for zero root water uptake at $z \geq z_m$, to account for nonsymmetrical root water uptake with depth and to allow for maximum root water uptake at any depth, z^{max} ($0 \leq z^{max} \leq z_m$). The nonsymmetry in root water uptake with soil depth is determined by the ratio between p_z for $z \leq z^*$, and the p_z value for $z > z^*$. To reduce the number of parameters, p_z is set to unity for values of $z > z^*$, whereas it is a fitted value for $z \leq z^*$. The value of $z = z^{max}$ can be calculated from the first derivative, i.e., $d\beta/dz = 0$.

As the potential cumulative root water uptake must equal the potential transpiration rate (T_{pot}), the normalized root water uptake distribution, S_m (T^{-1}), with depth is computed
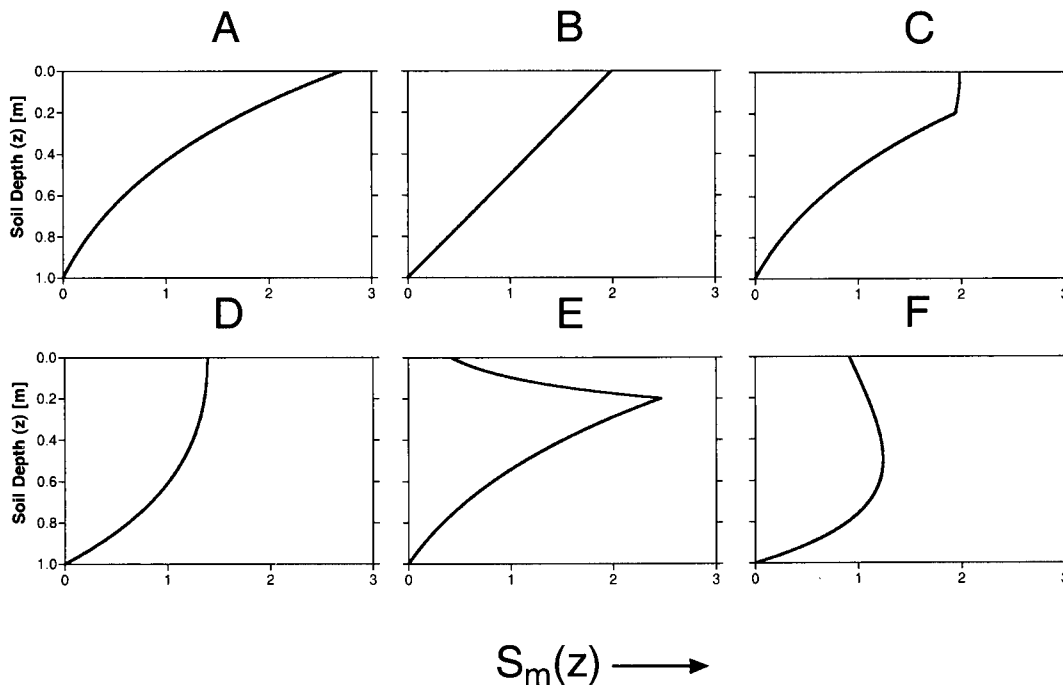

Fig. 1. Representation of different root water uptake models, $S_m(z)$, with depth.

from

$$S_{\mathrm{m}}(z) = \frac{\beta(z)T_{\mathrm{pot}}}{\displaystyle\int_{z=0}^{z=z_{\mathrm{m}}} \beta(z)\mathrm{d}z} \qquad [4]$$

Since in most field studies, z_{m} is known a priori, the uptake model of Eq. [3] contains only two unknown parameters (p_z and z^*). Figure 1 shows six different possible configurations of normalized root water uptake distribution, using z_{m} equals 1.0 m. The corresponding parameter values for the different models are listed in Table 1. The first four root water uptake models (A, B, C, and D) have maximum root water uptake at the soil surface ($z_{\mathrm{max}} = 0$), whereas the other two uptake distributions (E and F) simulate maximum uptake at z_{max} values of 0.2 and 0.5 m, respectively, as may be caused by subsurface drip irrigation.

For the characterization of the uptake intensity along the radial direction we used a similar expression as Eq. [3];

$$\beta(r) = \left[1 - \frac{r}{r_{\mathrm{m}}}\right]e^{-\frac{p_{\mathrm{r}}}{r_{\mathrm{m}}}|r^*-r|}; \qquad r \geq 0 \qquad [5]$$

where $\beta(r)$ characterizes the dimensionless spatial distribution of unstressed root water uptake in the r direction; r_{m} is the maximum rooting length in the radial direction (L); r is the radial distance from the origin of the plant (L) and p_{r} and r^* are empirical parameters with units (-) and (L), respectively. As in Eq. [3] we set p_{r} to unity for $r > r^*$.

Combining the uptake intensity along the z-direction (Eq. [3]) with the uptake intensity along the radial direction leads

Table 1. Parameter values for different water uptake distributions under nonstress conditions.

Model	Literature (adapted from)	z^*	p_z
		m	-
A	Raats, 1974	0.00	-†
B	Prasad, 1988	1.00	0.01
C	Hoffman and van Genuchten, 1983	0.20	1.00
D		0.20	10.0
E		1.00	1.00
F		1.00	2.00

† Model does not include parameter similar to p_z.

to a two-dimensional root water uptake model, which can be expressed as

$$\beta(r,z) = \left[\left(1 - \frac{z}{z_{\mathrm{m}}}\right)\right]\left[\left(1 - \frac{r}{r_{\mathrm{m}}}\right)\right]e^{-\left(\frac{p_z}{z_{\mathrm{m}}}|z^*-z|+\frac{p_{\mathrm{r}}}{r_{\mathrm{m}}}|r^*-r|\right)} \qquad [6]$$

where $\beta(r,z)$ denotes the dimensionless two-dimensional spatial distribution of root water uptake.

Both the presented water uptake model and the bivariate gaussian density functions presented by Coelho and Or (1996) contain six parameters. However, the proposed model includes at least two parameters (z_{m} and r_{m}) with a physical meaning. In contrast to the model of Coelho and Or (1996), Eq. [6] can be directly evaluated in the limit as $z \rightarrow 0$ and $r \rightarrow 0$. The single expression of Eq. [6] can simulate a wide variety of root water uptake patterns, whereas Coelho and Or (1996) introduce different distribution functions that need to be evaluated between uptake patterns.

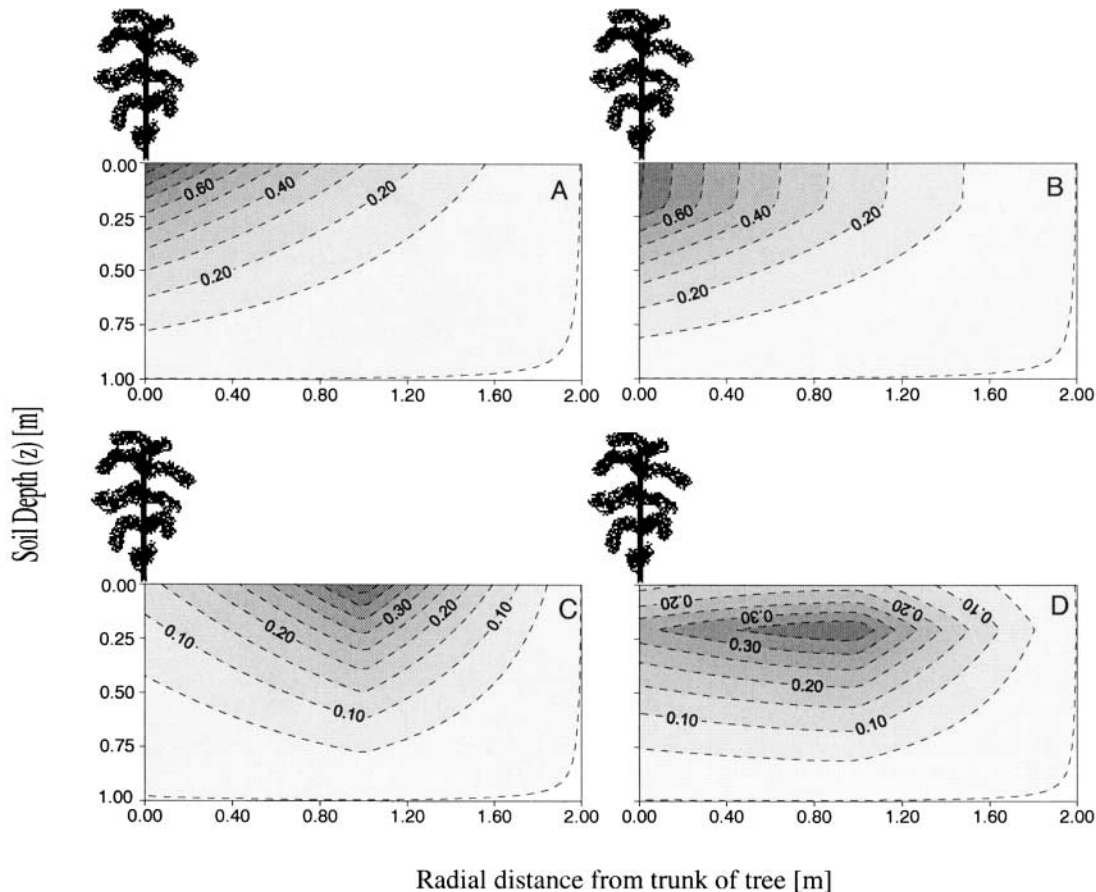Denoting the normalized root water uptake, S_{m}, as the vol-

Fig. 2. Four different configurations of two-dimensional spatial distribution of potential root water uptake, $\beta(r,z)$.

Table 2. Parameter values for the two-dimensional root water uptake configurations in Fig. 2.

Figure	fitting parameters						derived	
	z_m	r_m	z^*	r^*	p_z	p_r	z^{max}	r^{max}
	m				(-)			
A	1.00	2.00	0.00	0.00	1.00	1.00	0.00	0.00
B	1.00	2.00	0.20	0.00	1.00	1.00	0.20	0.00
C	1.00	2.00	0.00	1.00	1.00	4.00	0.00	1.00
D	1.00	2.00	0.20	1.00	5.00	2.00	0.20	1.00

ume of water extracted per unit time and volume of soil while assuming axial symmetry, it follows that (Šimunek et al., 1999)

$$S_m(r,z) = \frac{\pi R^2 \beta(r,z) \, T_{pot}}{2\pi \int\limits_0^{z_m} \int\limits_0^{r_m} r\beta(r,z)drdz} \qquad [7]$$

where $S_m(r,z)$ denotes the normalized root water uptake rate (T^{-1}) and R is the size of the flow domain in the r-direction. If $r_m < R$ then the value of R in Eq. [7] automatically equals r_m.

Four different types of two-dimensional root water uptake patterns for unstressed conditions are presented in Fig. 2, which were simulated with the proposed model in Eq. [6]. The corresponding parameters of the different water uptake distributions are listed in Table 2. A root water uptake intensity pattern as presented in Fig. 2a,b is expected for uniform water application. Much different uptake patterns are shown in Fig. 2c (surface irrigation) and Fig. 2d (subsurface irrigation), where the location of maximum uptake intensity shifts to locations with maximum irrigation application rate for nonuniform water applications. The proposed root water uptake model can be easily extended to three dimensions by including an additional exponential term in Eq. [6]. Moreover, the model can be adapted to account for root growth by allowing time-dependent z_m and r_m values during a growing season.

To provide for root water uptake under water-stressed conditions, a soil water stress response function was included (van Genuchten, 1987).

$$\gamma(r,z,h) = \frac{1}{\left[1 + \left(\dfrac{h}{h_{50}}\right)^p\right]} \qquad [8]$$

where h is the soil water pressure head at spatial location (r, z); h_{50} is the soil water pressure head (L) at which root water uptake rate is reduced by 50%; and p is a fitting parameter (-). The parameter p is usually assumed to be 3 (van Genuchten and Gupta, 1993).

Finally, the actual root water uptake rate at (r,z) can be calculated from

$$S(h,r,z) = \gamma(r,z,h)S_m(r,z) \qquad [9a]$$

and

$$T_{pot} = K_c ET_0 - E_s \qquad [9b]$$

where $S(h,r,z)$ is the actual water uptake (T^{-1}); K_c is the crop coefficient (-); ET_0 is the reference evapotranspiration (LT^{-1}); and E_s denotes soil evaporation (LT^{-1}). Hence, the actual transpiration rate (T_a) can be computed from Eq. [10].

$$T_a = \frac{2\pi}{\pi R^2} \int\limits_0^{z_m} \int\limits_0^{r_m} rS(h,r,z)drdz \qquad [10]$$

Field Description and Measurements

The experimental plot is located in an almond orchard, and covers about one quarter of the wetted area of a microsprinkler irrigating a single almond tree (Koumanov et al., 1997). In the 2.0 m by 2.0 m instrumented area, 25 polyvinyl chloride neutron probe access tubes were installed in a square grid of 0.50 m spacing to a depth of 90 cm (Fig. 3). The neutron probe was calibrated from gravimetric measurements using soil samples collected at soil depths of 15, 30, 45, 60, 75, and 90 cm during and after access tube installation. Separate calibration curves were used for the 0- to 15-cm surface soil and the 30- to 90-cm soil depth interval. Standard errors of estimate of volumetric water content curves were approximately 0.01 (15 cm depth interval) and 0.02 m³ m⁻³ (all other measurements
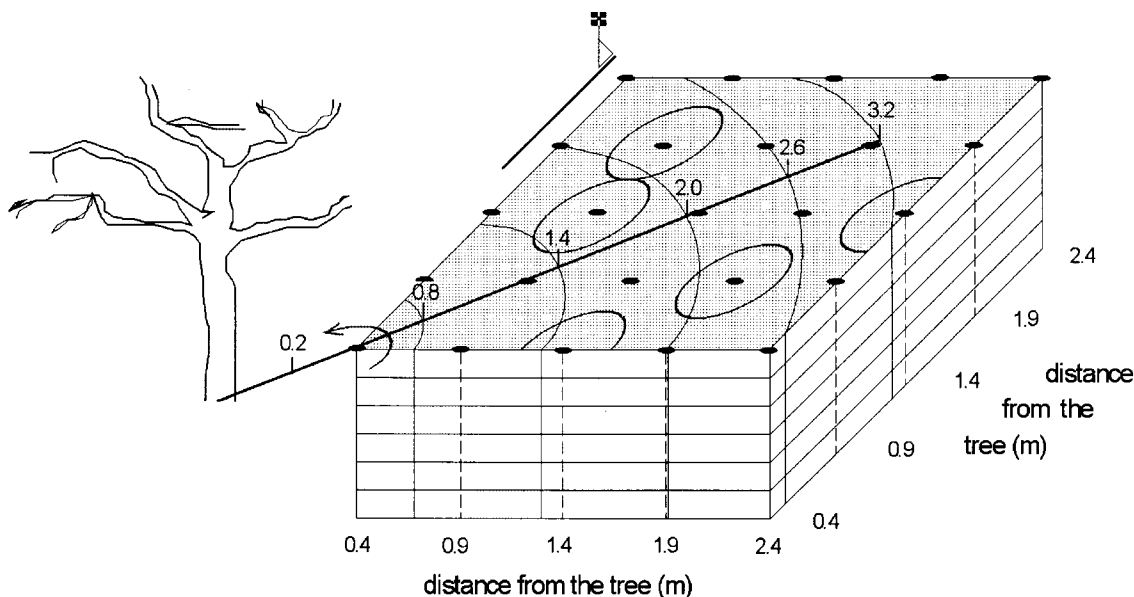

Fig. 3. Schematic view of the experimental plot (after Koumanov et al., 1997).

depths). The field is slightly undulating, and the soil is a shallow gravely loam (Andreu et al., 1997), overlaying a sloping high density restricting clay layer at about the 90- to 120-cm soil depth. The study by Andreu et al. (1997) indicated that root water uptake during the growing season was mainly limited to the top 60 cm, and that drainage of the soil primarily occurred by lateral flow along the sloping restricting clay layer.

The measurements were carried out 13 September through 29 September in the summer of 1995. First, the sprinkler system was used to moisten the whole soil profile. Neutron probe measurements were taken on 13 September, immediately after the irrigation at 1300, 1500, and 1800 h, during the period of 14 September through 17 September, every 4 h at 600, 1000, 1400, and 1800 h, and during the period of 18 September through 29 September, daily at ~1000 h.

To simplify testing of the root water uptake model, the three dimensional grid measurements of water content needed to be reduced to two dimensions (r and z). For this we assumed that (i) the root water uptake around the tree was axisymmetrical and (ii) that the measurement volume of the neutron probe water content was a sphere with a constant radius of ~0.25 m. Although the first assumption was rather arbitrary, there was no reason to expect the contrary.

First, for each depth interval the rectangular measurement grid of Fig. 3 was partitioned into five concentric adjacent 0.6-m wide circular strips with the origin of the circles defining these soil strips. The soil strips were determined by the neutron access pipe location closest to the tree trunk (see Fig. 3). Second, a radial-average water content value was computed for each of the five soil areas (0.2–0.8, 0.8–1.4, 1.4–2.0, 2.0–2.6, and 2.6–3.2 m) using weighting factors for each neutron probe location with values equal to the fraction of the measurement volume fitting within the respective concentric soil area. We used 0.6 m wide strips for each of the five soil areas to ensure that enough water content measurements were contained within the respective strip. Moreover, the averaging using the 0.6-m wide strips gave the best agreement in total water depletion of the reduced two-dimensional domain as compared to the original three-dimensional grid of water content measurements. Since the averaging procedure was applied to depth intervals of 0 to 0.15, 0.15 to 0.3, 0.3 to 0.45, and 0.45 to 0.6, the final two-dimensional map included 20 average water content values at each measurement time (four depth intervals and five radial distance increments) during the 13 September to 29 September calibration period.

Water Flow Simulation

While assuming axial symmetry for an isotropic soil, the Richards equation for a rigid porous media can be written as (Inoue et al., 1998; Šimůnek et al., 1999)

$$C \frac{\partial h}{\partial t} = \frac{1}{r} \frac{\partial}{\partial r}\left(rK\frac{\partial h}{\partial r}\right) + \frac{\partial}{\partial z}\left(K\frac{\partial h}{\partial z}\right) - \frac{\partial K}{\partial z} - S(h,r,z)$$

[11]

where C is the water capacity (L^{-1}); h is the soil water pressure head (L); r is the radial coordinate; z is the vertical coordinate (positive downwards); t is time (T); and $S(h,r,z)$ denotes root water uptake (T^{-1}). Equation [11] was solved with the HYDRUS–2D model (Šimůnek et al., 1999) using the Galerkin finite element method based on the mass conservative iterative scheme proposed by Celia et al. (1990).

The unsaturated hydraulic properties in HYDRUS–2D are defined by (van Genuchten, 1980; Mualem, 1976)

$$\frac{\theta - \theta_r}{\theta_s - \theta_r} = S_e = [1 + (-\alpha h)^n]^{-m}; \quad m = \frac{n-1}{n}$$

[12]

and

$$K(S_e) = K_s S_e^l \left\{ 1 - \left[1 - S_e^{(1/m)}\right]^m \right\}^2$$

[13]

where θ_s is the saturated water content ($L^3\ L^{-3}$); θ_r is the residual water content ($L^3\ L^{-3}$); $\alpha(L^{-1})$, n, and l are curve shape parameters (-); and K_s is the saturated hydraulic conductivity (L T^{-1}). The simulated flow domain was 3.0 m long (radial direction) by 0.6 m deep, using a grid spacing of 0.05 m in the radial and 0.05 m in the vertical direction.

Boundary and Initial Conditions

For the soil surface boundary conditions, HYDRUS–2D requires estimates of the potential transpiration (T_{pot}) and soil evaporation (E_s). Daily reference evapotranspiration (ET_0) data was provided by a nearby weather station of the California Irrigation Management Information System (CIMIS). Almond potential ET_{alm} was calculated from ET_0 and the appropriate crop coefficients (K_c). Snyder et al. (1988) recommended a value for K_c of 0.91, corresponding to conditions of 60% canopy soil surface coverage for drip-irrigated trees in the Sacramento Valley. Ritchie's (1972) equation was used to estimate soil evaporation. The radiation interception was calculated using the empirical function for maize (*Zea mays* L.) (Snyder et al., 1985), while we used an upper limit of Stage 1 cumulative evaporation of 6 mm and a partitioning factor of 0.4 between Stage 1 and Stage 2 evaporation (Ritchie, 1972). The potential transpiration of almond trees (T_{alm}) was obtained by subtracting E_s from ET (Eq. [9b]). Figure 4 presents the daily boundary conditions as functions of time during the monitoring period that were used for the HYDRUS–2D model simulations.

Due to the lack of flux information, we assumed a unit hydraulic gradient as the lower boundary condition (gravity flow). The calculated two-dimensional soil moisture profile immediately after irrigation, 13 September, was used as initial condition for the numerical simulations.

Parameter Optimization

In addition to the root water uptake parameters z_m, r_m, z^*, r^*, p_z and p_r (Eq. [6]), and the stress response parameter h_{50} (Eq. [8]), the soil hydraulic parameters n and K_s were also optimized. Although the soil hydraulic properties of a nearby location in the same almond orchard were reported by Andreu et al. (1997), the large soil heterogeneity within the orchard made it necessary to also optimize the soil hydraulic parameters simultaneously with the root water uptake model parame-
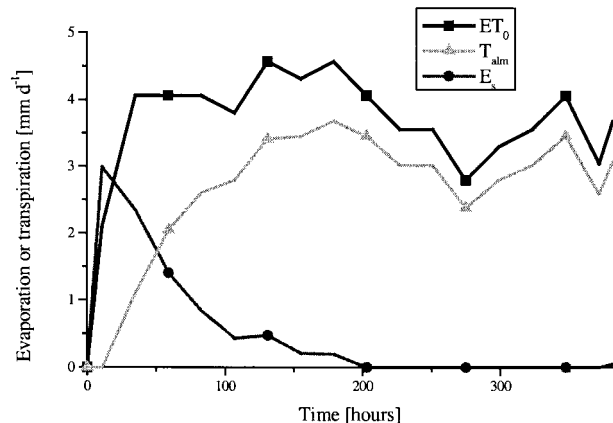

Fig. 4. Soil surface boundary conditions during simulation period (Time 0 corresponds with 13 September).

ters. While fixing the parameters θ_s, θ_r, α, and l to reported values of 0.28, 0.0, 9.4 m^{-1}, and −0.850, respectively (Andreu et al., 1997), spatial variability in soil hydraulic properties was assumed to be characterized by the fitting parameters n and K_s (Eq. [12] and [13]). We fixed the parameters θ_s, θ_r, α, and l to their reported values to partly avoid problems with nonuniqueness of the parameter estimates, especially because a relatively large number of root parameters are already involved in the optimization. Hence, in the calibration stage of this study, a combined total of nine root water uptake and soil hydraulic parameters were optimized simultaneously.

Since optimization algorithms such as Levenberg–Marquardt or Simplex method are only generally applicable to identify a limited number of unique parameters, an alternative was needed to optimize this many parameters. Recently it has been shown that GAs are a powerful tool for parameter identification, when the number of fitted parameters is large (Bäck, 1996; Holland, 1975). Genetic algorithms were developed in evolution theory, based on the concepts of natural selection and genetics. In this approach, variables are represented as genes on a chromosome. Genetic Algorithms feature a group of candidate solutions (population) on a response surface. Through natural selection and using genetic operators, such as mutation and crossover, the objective of a GA is to search for chromosomes with improved fitness, that is, a parameter set, which is closer to the global optimum in the objective function. Natural selection guarantees that chromosomes with the best fitness will propagate in future populations. Using the crossover operator, the GA combines genes from two parent chromosomes to form new chromosomes (children) that have a high probability of having better fitness than their parents. Mutation allows near areas of the response surface to be explored. Hence, GAs offer an improvement in the fitness of the chromosomes through application of the GA in reproduction, so that many generations will create chromosomes containing the optimized variable settings (Wang, 1991).

We applied the GA method presented in Penny and Lindfield (1995), with the small adaptation that the best performing parameter combination is not mutated in the next generation. We used a relatively high crossover value of 0.85 to ensure a relatively fast convergence to the global optimum, where as a mutation factor of 0.15 was used to avoid optimized solutions in local minima. The population size or number of possible first generation parameter combinations was set to 150, whereas the final selected optimized parameter combination was determined after 100 generations. The fitness of a chromosome was calculated by:

$$OF(b) = \sum_{i=1}^{n} [\theta^*(t_i) - \theta(t_i,\mathbf{b})]^2 \qquad [14]$$

where n is the number of measurements; and $\theta^*(t_i)$ and $\theta(t_i,\mathbf{b})$ denote the measured and predicted water content values, respectively, at time t_i. The parameter vector, $\mathbf{b}$, characterizes the chromosome with the genes representing the fitting parameters. The lower the value of objective function, OF($\mathbf{b}$), the more fit is the chromosome. The allowable ranges of the parameters included in $\mathbf{b}$ are presented in Table 3 and are determined by physical constraints of possible parameter values.

Table 3. Range parameters values used in global optimization with genetic algorithms.

	Parameter								
	z_m	r_m	z^*	r^*	p_z	p_r	h_{50}	n	K_s
			m		(-)		m	-	m d^{-1}
Min	0.00	0.00	0.00	0.00	0.10	0.10	−0.30	1.2	1e-4
Max	0.60	5.00	0.60	5.00	15.0	15.0	−50.0	4.0	0.64

Although GAs are an effective means of determining the global minimum region, their use is not necessarily the most efficient way of finding the exact optimum location. Therefore, the results of the GA were used as initial values for the Simplex optimization to determine the local minimum of Eq. [15] within the global minimum region. Using a sensitivity analysis in which each parameter was varied by 10% around its true value, while keeping the additional parameters fixed at their value found by the GA, we selected those six parameters in the parameter vector that were most sensitive to the model output. Both the GAs and the simplex optimization were carried out using MATLAB, version 5.3 (The Mathworks, 1999). The estimated standard deviation of each parameter b_j of $\mathbf{b}$ was determined from the diagonal elements of the parameter covariance matrix C (Kool and Parker, 1988),

$$s_j = \sqrt{C_{jj}} \qquad [15]$$

whereas final fitting results were expressed as RMSE values, computed from

$$RMSE = \sqrt{\frac{\sum_{i=1}^{n} [\theta^*(t_i) - \theta(t_i,\mathbf{b})]^2}{n - m}} \qquad [16]$$

where m is the total number of parameters.

RESULTS AND DISCUSSION

Final parameter values after performing the GA and the Simplex optimization are presented in Table 4. This table also includes final derived parameter values, such as z^{max}, r^{max}, and the 95% confidence intervals using the residuals and Jacobian matrix at the final solution. The fitting results are expressed by RMSE values. As the parameters z_m, r_m, z^*, r^*, n, and K_s showed the highest sensitivity to the model output in the parameter solution obtained with the GA, these six parameters were further optimized using the SA. Because of the simultaneous fitting of this many parameters, problems may occur with the nonuniqueness of the parameter estimates

Table 4. Optimized parameter values after genetic algorithm (GA) and Simplex algorithm (SA). Also included are the 95% parameter confidence intervals of the final solution and the coefficient of variation of the final parameter estimates.

Parameter		GA	SA	95% Confidence interval Lower	Upper	CV
						%
z_{zm}	(m)	0.426	0.403	0.326	0.481	9.6
r_m	(m)	4.174	4.144	3.463	4.825	8.3
p_z	(-)	3.214	†	2.319	4.109	13.9
p_r	(-)	2.918	†	2.412	3.424	8.7
z^*	(m)	0.300	0.330	0.189	0.469	21.2
r^*	(m)	2.052	2.075	1.862	2.288	5.1
n	(-)	1.673	1.674	1.545	1.803	3.9
K_s	(cm d^{-1})	0.408	0.460	0.350	0.569	11.9
h_{50}	(m)	−0.533	†	−0.733	−0.333	18.7
RMSE	(m^3 m^{-3})	0.0157	0.0154			
R^2		0.91	0.92			
Derived Parameters						
z^{max}	(m)	0.294	0.278			
r^{max}	(m)	2.053	2.075			

† Open space indicates that parameter was held constant at value estimated by GA.

caused by the presence of multiple local minima in the objective function.

Since parameter estimation involves a variety of possible errors, including measurement, model and numerical errors, an uncertainty analysis of the optimized parameters constitutes an important part of parameter estimation. Table 4 shows that the standard deviations of the various parameters are typically small, revealing that the information of the water content measurements for most of the parameters is robust (e.g., Vrugt et al., 2001). Although a variety of errors determine the final parameter standard deviation, the root parameters p_z and z^*, have a relatively higher uncertainty as compared to the other root parameters. Their larger values of the coefficient of variation (CV), may be caused by the smaller number of nodal points defining a strip in the depth direction as compared to the radial direction. Furthermore, the 95% confidence interval of the n-parameter in the soil hydraulic functions lies within the range of n-values between 1.44 and 1.99 as reported by Andreu et al. (1997) at a nearby location between the 0- and 60-cm depth. The relatively high uncertainty in h_{50} as indicated by its CV value, is partly because of its extreme large value, corresponding with a low water holding capacity of this soil. Although not presented, inspection of the parameter correlation matrix for the final solution showed that correlations between the parameter estimates are typically low ($R < 0.50$), except between parameter r_m and z^* ($R = -0.88$), r_m and r^* ($R = 0.92$), z^* and r^* ($R = 0.88$), and n with K_s (0.88).

The optimized soil water retention and unsaturated soil hydraulic conductivity curves from the final SA solution are presented in Figure 5. Also included are the measured (θ,h) data using the multistep outflow method from soil cores taken at a 30-cm depth at a nearby location, and (K,θ) points as obtained using the instantaneous profile method at a nearby location at the 30-cm soil depth (Andreu et al., 1997). Both the measured (θ,h) points and the optimized retention curve clearly show the small water holding capacity of this shallow gravely soil. Additionally, the optimized unsaturated hydraulic conductivity and measured (K,θ) points show the rapid decrease of the hydraulic conductivity with decreasing water content. Moreover, the large soil water stress value ($h_{50} = -0.53$ m) is in agreement with the low water holding capacity of this soil. The optimized saturated conductivity of 0.46 cm d^{-1} of the SA optimization is much lower than the reported range of 34.1 to 62.4 cm d^{-1} between 0- and 60-cm depth by Andreu et al., 1997. However, one should realize that the saturated hydraulic conductivity in this study, is much more a water balance parameter controlling the magnitude of the lower boundary flux than it is a soil physical parameter affecting soil water flow in the soil domain.

The range of the maximum rooting depth (z_m) as found by the SA (0.33 m < z_m < 0.48 m) is in excellent agreement with the results obtained by Koumanov et al. (1997) for the same experimental plot, suggesting that active root water uptake was limited to the top 40 cm only using seasonal root and soil water content
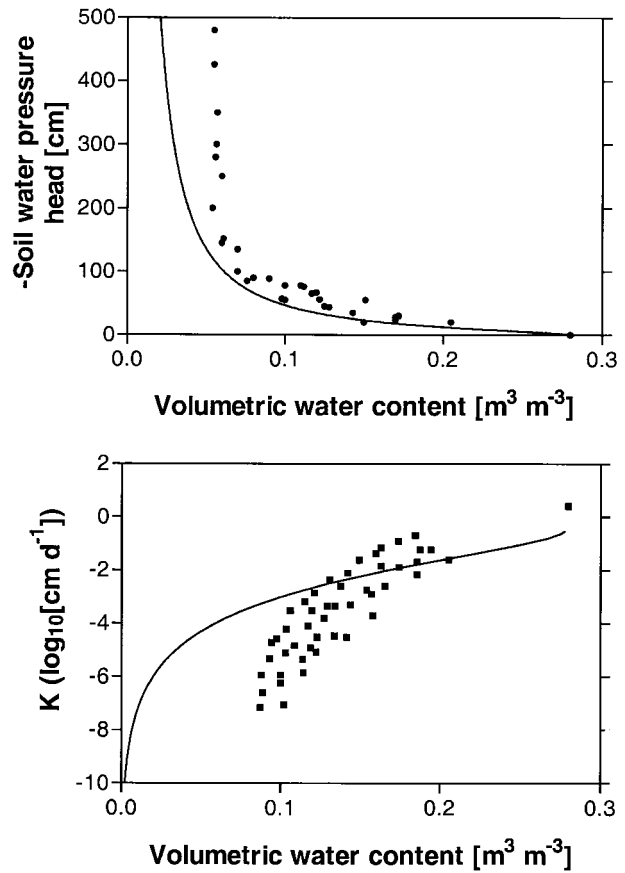

Fig. 5. Optimized soil water retention and unsaturated hydraulic conductivity curves as obtained by the Simplex Algorithm optimization and measured (θ,h) using the multistep outflow method from soil cores taken at 30-cm depth at a nearby location and (K,θ) points, as obtained using the instantaneous profile method at a nearby location for the 30-cm soil depth.

observations. Whereas our optimization results indicate the depth of maximum root water uptake is about 0.28 m, the study by Andreu et al. (1997) concluded that maximum uptake occurred at the soil surface (0–15 cm) and decreased further down the soil profile. However, their study did not include soil evaporation as a possible mechanism of soil water depletion near the soil surface. The optimized radial position of maximum root water uptake (r^{max}) of the almond tree (2.07 m) agreed well with the region of highest irrigation application amounts of the microsprinkler (Koumanov et al., 1997). This was so, despite the location of the microsprinkler at the far corner along the tree row (see Fig. 3), and was caused by systematic nonuniform water applications during the irrigation period. This finding is consistent with the experimental data of Coelho and Or (1996), who concluded that the applied irrigation strategy can determine root development in both space and time.

Figure 6 presents the optimized spatially distributed root water uptake model, $\beta(r,z)$, as determined over the 16-d monitoring period using the final optimized root water uptake parameters. Clearly, the zone of maximum root water uptake is concentrated in a thin soil layer between 0.1 and 0.35 m. In this area, the roots act like a sink and provide for soil water potential differ-
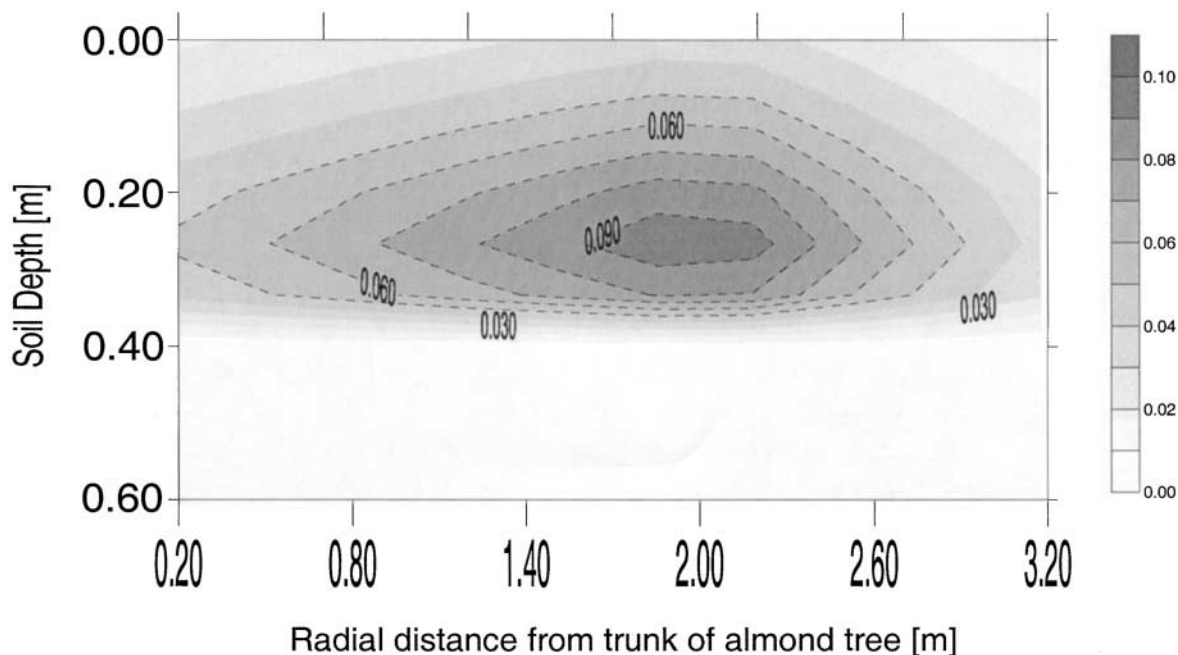
Fig. 6. Optimized spatial distribution of potential transpiration β(r,z).

ences in the soil that regulate soil water flow towards this active soil region from above and below.

For calibration purposes, the two-dimensional flow region of the rooting zone of the single tree was divided into 20 blocks of 0.6 by 0.15 m. The residuals in volumetric water content of only 12 of these blocks (C1–12) were included in the OF (Eq. 14), and served as calibration values. The eight remaining blocks are used for validation (V1–8). Measured and simulated average water content values for all 20 blocks as a function of time are presented in Fig. 7. The position of the graphs indicates the position of each block in the two-dimensional plane. Although simulated water contents using the optimized soil hydraulic and root water uptake parameters agree remarkably well with measured water content values, there are some discrepancies. For instance, simulated and measured water content values deviate considerably for blocks C7 and V6. Clearly, the presented procedure includes restrictive assumptions, making a perfect fit unlikely. For example, we have assumed that root water uptake is axisymmetrical. The original three-dimensional measured water content values, however, showed that this can only be approximately true. Moreover, the root water uptake model

assumes that only a single region of maximum water uptake exists, whereas multiple regions within a rooting system may show maximum uptake as caused by nonuniform water application and soil environmental factors affecting root growth.

The explained variances and time-averaged RMSE between measured and optimized water content values for all calibration and verification blocks of the monitoring period are presented in Table 5. The overall fit, as computed from the RMSE values is excellent, considering that the standard error of the water content measurements with the neutron probe is between 0.01 m^3 m^{-3} (15-cm depth) and 0.02 m^3 m^{-3} (all larger depths).

The final two-dimensional maps of simulated water content (m^3 m^{-3}) with corresponding root water uptake intensity (m^3 m^{-3} h^{-1}) at three times during the calibration period are shown in Fig. 8, and were obtained from interpolation of nodal values using SURFER (Golden Software, 1996). At the beginning of this period, maximum water uptake rates approached 7.0×10^{-4} m^3 m^{-3} h^{-1}. As these soil volumes become depleted in water, regions of maximum root water uptake shift to other locations within the rooting zone where soil water is more readily available. For example, close observation

Table 5. Final optimization results for both calibration (C) and validation (V) blocks.

| | Subregion | | | | | | | | | | | |
	C1	C2	C3	C4	C5	C6	C7	C8	C9	C10	C11	C12
RMSE	0.012	0.015	0.006	0.011	0.015	0.008	0.036	0.014	0.008	0.011	0.017	0.011
R^2	0.98	0.95	0.99	0.99	0.99	0.99	0.54	0.98	0.99	0.99	0.90	1.00

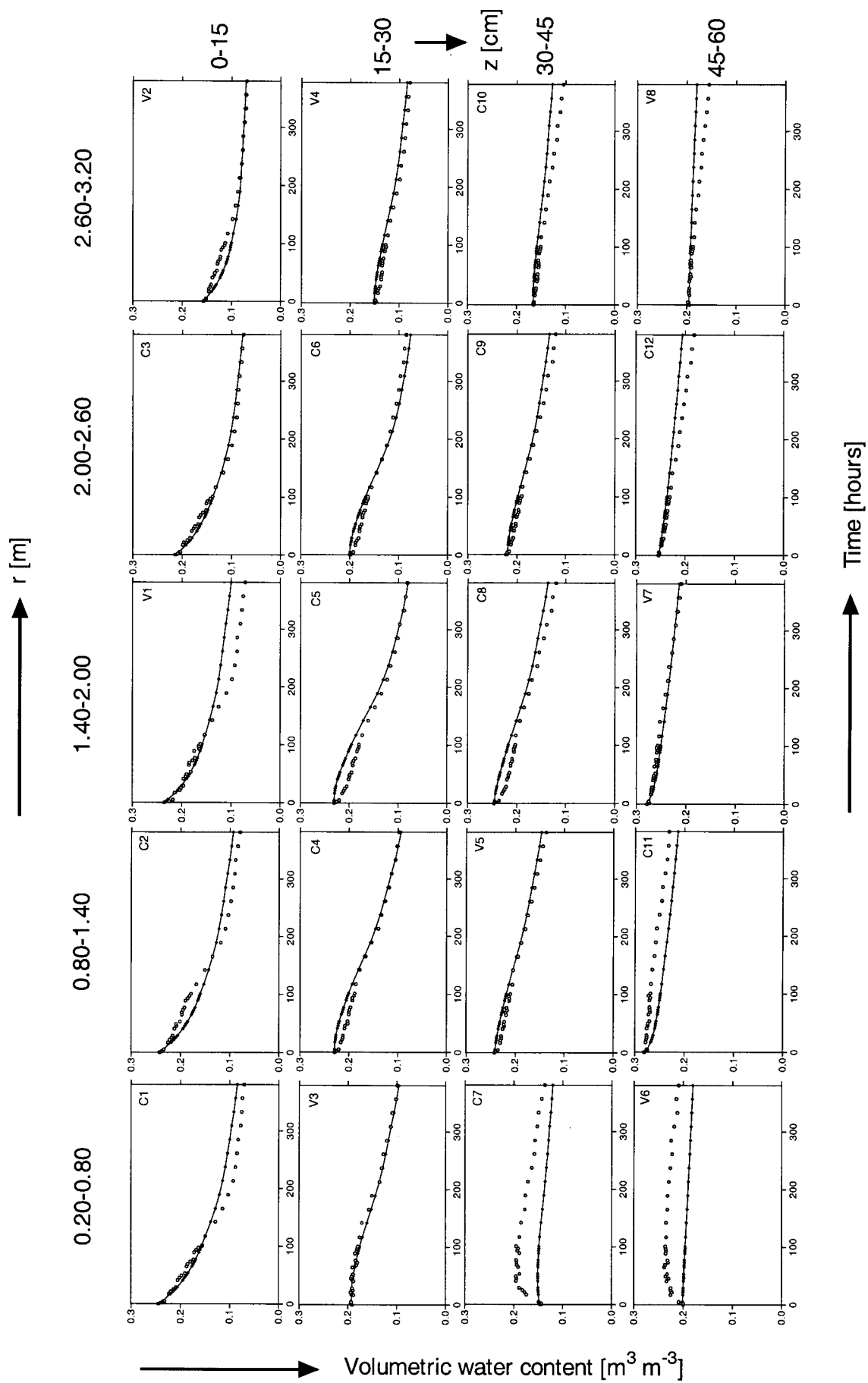| | Subregion | | | | | | | | |
	V1	V2	V3	V4	V5	V6	V7	V8	Overall
RMSE	0.016	0.010	0.004	0.007	0.008	0.034	0.004	0.011	0.0154
R^2	0.95	0.94	0.99	0.99	0.99	0.05	0.97	1.00	0.92

Fig. 7. Measured (open circles) and simulated (solid lines) water content values as a function of time across the measured spatial domain of the almond tree (C denotes calibration and V is validation).
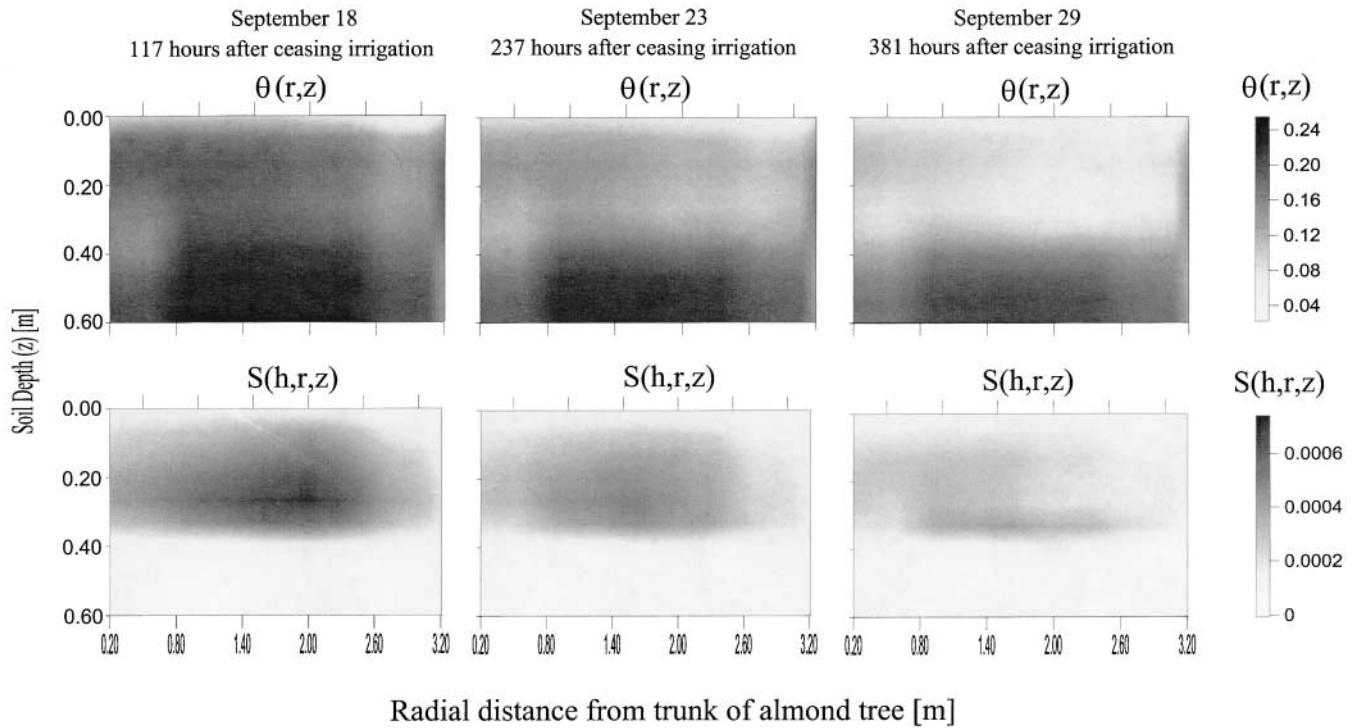
Fig. 8. Two-dimensional maps of simulated water content values (m³ m⁻³) and root water uptake (d⁻¹) at three different times during the experimental period.

of Fig. 8 shows that root water uptake patterns change with time towards regions further away from the center of the initial highest water uptake

Finally, in Fig. 9a, we present the different components of the soil water balance as calculated by the HYDRUS–2D model. The total simulated change in soil water storage of the axial symmetric two-dimensional grid during the period 13 September through 29 September was 1692 L, which corresponds to a soil water depletion of 52.8 mm for the 0.6 by 3.0 m soil domain. Soil evaporation (13.2%) and root water uptake (69.7%) account for 82.9% of the total soil water storage change, whereas the remaining depletion (17.1%) is caused by drainage. The difference between cumulative root water uptake and cumulative potential transpiration is caused by soil water stress, which mainly occurs

at the end of the study period, as the rooting zone becomes further depleted of water. Over the whole domain during the experimental period, the reduction in transpiration for T_{pot} is 23.5%, with the difference between potential and actual evapotranspiration being about 11 mm. Although soil water storage is not explicitly included in the objective function, there was excellent agreement between measured and simulated soil water depletion, as shown in Fig. 9b.

CONCLUSIONS

In this paper we have presented a two-dimensional root water uptake model which was based on the model by Raats (1974). The developed root water uptake model is extremely flexible and allows spatial and tem-
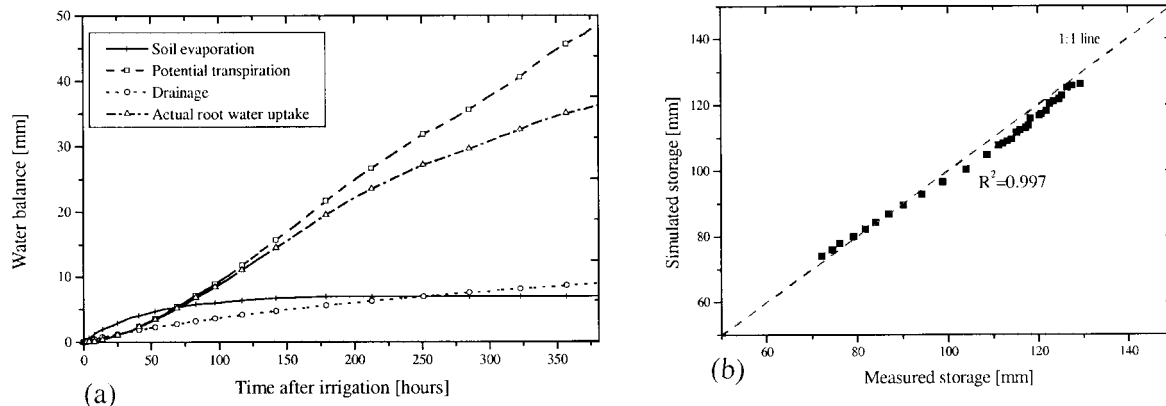

Fig. 9. (a) Components of the water balance, (b) Measured versus simulated soil water storage during the monitoring period.

poral variations of water uptake as influenced by uniform and nonuniform water application patterns. Using the optimized flow and uptake parameters, the simulated and measured water contents values during the 16-d period were in excellent agreement, with R^2 generally ranging between 0.94 and 0.99, and an average deviation of $0.015\ \mathrm{m^3\,m^{-3}}$. These results are excellent bearing in mind that the standard error of the water content measurements was between 0.01 m^3 m^{-3} and 0.02 m^{-3} m^{-3}. Some of the optimized root water uptake parameters such as maximum rooting depth agreed well with experimental observations in the same experimental plot. The relatively high value of the optimized soil water stress parameter agrees with the low water holding capacity of the gravely soil. Maximum root water uptake rates approached $7.0 \times 10^{-4}\ \mathrm{m^3\,m^{-3}\,h^{-1}}$, with soil regions of maximum root water uptake shifting to other locations within the rooting zone where soil water is more readily available.

ACKNOWLEDGMENTS

REFERENCES

Andreu, L., J.W. Hopmans, and L.J. Schwankl. 1997. Spatial and temporal distribution of soil water balance for a drip-irrigated almond tree. Agric. Water Manage. 35:123–146.

Bäck, T. 1996. Evolutionary algorithms in theory and practice: Evolution strategies, evolutionary programming, genetic algorithms. Oxford University Press, New York, NY.

Canadell, J., R.B. Jackson, J.R. Ehleringer, H.A. Mooney, O.E. Sala, and E.D. Schulze. 1996. Maximum rooting depth of vegetation types at the global scale. Oecologia 108:583–595.

Celia, M.A., E.T. Bouloutas, and R.L. Zarba. 1990. A general mass-conservative numerical solution for the unsaturated flow equation. Water Resour. Res. 26:1483–1496.

Clothier, B.E., and S.R. Green. 1994. Rootzone processes and the efficient use of irrigation water. Agric. Water Manage. 25:1–12.

Coelho, F.E., and D. Or. 1996. A parametric model for two-dimensional water uptake intensity by corn roots under drip irrigation. Soil Sci. Soc. Am. J. 60:1039–1049.

Clausnitzer, V., and J.W. Hopmans. 1994. Simultaneous modeling of transient three-dimensional root growth and soil water flow. Plant Soil 164:299–314.

Feddes, R.A., E. Bresler, and S.P. Neuman. 1974. Field test of a modified numerical model for water uptake by root systems. Water Resour. Res. 10:1199–1205.

Golden Software. 1996. Surfer, version 6.04c. Golden Software, Golden, CO.

Holland, J.H. 1975. Adaptation in natural and artificial systems. The University of Michigan Press, Ann Arbor, MI.

Hoffman, G.J., and M.Th. van Genuchten. 1983. Soil properties and efficient water use: Water management for salinity control. p. 73–85. In H.M. Taylor et al. (eds) Limitation to efficient water use in crop production. Am. Soc. Agron., Madison, WI.

Homaee, M. 1999. Root water uptake under non-uniform transient salinity and water stress. Ph.D. thesis. Agricultural University Wageningen, the Netherlands.

Inoue, M., J. Šimunek, J.W. Hopmans, and V. Clausnitzer. 1998. In situ estimation of soil hydraulic functions using a multistep soil-water extraction technique. Water Resourc. Res. 34:1035–1050.

Jarvis, N.J. 1989. A simple empirical model of root water uptake. J. Hydrol. 107:57–72.

Kool, J.B., and J.C. Parker. 1988. Analysis of the inverse problem for transient unsaturated flow. Water Resour. Res. 24:817–830.

Koumanov, K.S., J.W. Hopmans, L.J. Schwankl, L. Andreu, and A. Tuli. 1997. Application efficiency of micro-sprinkler irrigation of almond trees. Agric. Water Manage. 34:247–263.

The Mathworks. 1994. MATLAB, version 4.2.c. The Mathworks, Natick, MA.

Molz, F. 1981. Models of water transport in the soil-plant system: A review. Water Resour. Res. 17:1245–1260.

Mualem, Y.A. 1976. A new model for predicting the hydraulic conductivity of unsaturated porous media. Water Resour. Res. 12:513–522.

Musters, P.A.D. 1998. Temporal and spatial patterns of root water uptake in an Austrian pine stand on sandy soil. Ph.D. thesis. University of Amsterdam, the Netherlands.

Musters, P.A.D., and W. Bouten. 1999. Assessing rooting depths of an Austrian Pine stand by inverse modeling soil water content maps. Water Resour. Res. 35:3041–3048.

Neuman, S.P., R.A. Feddes, and E. Bresler. 1975. Finite element analysis of two-dimensional flow in soil considering water uptake by roots: I. Theory. Soil Sci. Soc. Am. J. 35:224–230.

Penny, J., and G. Lindfield. 1995. Numerical methods using MATLAB. Ellsi Horwood, New York.

Prasad, R. 1988. A linear root water uptake model. J. Hydrol. 99:297–306.

Raats, P.A.C. 1974. Steady flows of water and salt in uniform soil profiles with plant roots. Soil Sci. Soc. Am. Proc. 38:717–722.

Ritchie, J.T. 1972. Model for predicting evaporation from a row crop with incomplete cover. Water Resour. Res. 8:1204–1212.

Šimunek, J., M. Šejna, and M.Th. van Genuchten. 1999. The HY-DRUS-2D software package for simulating two-dimensional movement of water, heat, and multiple solutes in variable saturated media. Version 2.0, IGWMC-TPS-53, International Ground Water Modeling Center, Colorado School of Mines, Golden, CO.

Snyder, R.L., and W.O. Pruitt. 1989. Crop coefficients. p. 67. In Goldhamer and Snyder (ed.) Irrigation scheduling—Aguide for efficient on-farm water management. Univer. of Calf. Div. Agric. Nat. Res. Publ. No. 21454.

Snyder, R.L., W.O. Pruitt, D.W. Henderson, and A. Dong. 1985. California irrigation management information system final report. Vol. I. Dept. Land, Air and Water Resourc., Univer. of Calif., Davis, CA.

Somma, F., J.W. Hopmans, and V. Clausnitzer. 1998. Transient three-dimensional modeling of soil water and solute transport with simultaneous root growth, root water and nutrient uptake. Plant Soil 202:281–293.

van Genuchten, M.Th. 1987. A numerical model for water and solute movement in and below the root zone. Res. Rep. 121. U.S. Salinity Lab, ARS USDA, Riverside, CA.

van Genuchten, M.Th., and S.K. Gupta. 1993. A reassessment of the crop tolerance reponse function. Indian Soc. Soil Sci. 4:730–737.

van Genuchten, M.Th. 1980. A closed-form equation for predicting the hydraulic conductivity of unsaturated soils. Soil Sci. Soc. Am. J. 44:892–898.

Vrugt, J.A., W. Bouten, and A.H. Weerts. 2001. Information content of data for identifying soil hydraulic parameters from Outflow experiments. Soil Sci. Soc. Am. J. 65:19–27.

Walton, B.T., and T.A. Anderson. 1990. Microbial degradation of trichloroethylene in the rhizosphere: Potential application to biological remediation of waste sites. Appl. and Environ. Biol. 56:1012–1016.

Wang, Q.J. 1991. The genetic Algorithm and its application to calibrating conceptual rainfall runoff models. Water Resour. Res. 27:2467–2471.

Warrick, A.W., D.O. Lomen, and A.A. Fard. 1980. Linearized moisture flow with root extraction for three dimensional, steady conditions. Soil Sci. Soc. Am. J. 44:911–914.

Whisler, F.D., A. Klute, and R.J. Millington. 1968. Analysis of steady state evapotranspiration from a soil column. Soil Sci. Soc. Am. Proc. 32:167–174.